HHS Public Access

Author manuscript

Methods Enzymol. Author manuscript; available in PMC 2019 February 04.

Published in final edited form as:

Methods Enzymol. 2015 ; 564: 485–497. doi:10.1016/bs.mie.2015.06.032.

Practical Aspects of Paramagnetic Relaxation Enhancement in Biological Macromolecules

G. Marius Clore*

Laboratory of Chemical Physics, Building 5, National Institute of Diabetes and Digestive and Kidney Diseases, National Institutes of Health, Bethesda, MD 20892-0520, U. S. A.

1. Introduction

The mainstay of classical macromolecular NMR structure determination resides in short (<6 Å) interproton distance restraints derived from nuclear Overhauser enhancement (NOE) measurements, supplemented by torsion angle restraints derived from three-bond homo- and heteronuclear scalar coupling constants (1). While this approach has been very successful, especially for globular proteins where there are a large number of short interproton distances between residues far apart in the linear amino acid sequence (1), long-range information can be extremely beneficial, especially in cases involving multidomain proteins, nucleic acids or macromolecular complexes (2–4). There are two source of long range information: the first is from residual dipolar couplings measured in weakly aligning media which provide bond vector orientations relative to an external alignment tensor (5); the second involves the application of paramagnetic relaxation enhancement (PRE) that can, in suitable cases, detect interactions between an unpaired electron of a paramagnetic site and protons up to ~35 Å away (6). In this brief review, I will summarize in non-mathematical terms various practical aspects of PRE measurements and show how the PRE can be used not only as an aid in structure determination, but perhaps even more interestingly, in the detection and characterization of transient sparsely-populated states of proteins and their complexes. The latter has garnered considerable recent interest as such sparsely-populated states, while invisible to conventional structural and biophysical methods (including crystallography, conventional NMR, cryo-electron microscopy, EPR and single molecule spectroscopy), often play a key role in a variety of important biological processes, including molecular recognition, allostery, conformational selection and induced fit, and various assembly processes (7–11). For an in-depth review of the PRE, including a detailed description of the underlying physics and mathematical representations, I refer the reader to several extensive reviews that have recently appeared on the use of the PRE in both structure determination and the investigation of sparsely-populated states (6, 12, 13).

The PRE arises from magnetic dipolar interactions between unpaired electrons in a paramagnetic center and a nucleus resulting in an increase in nuclear relaxation rates. The paramagnetic center can either be an intrinsic component of the system as in the case of metalloproteins, or an intrinsic component that has to be added by chemical means (such as

* mariusc@mail.nih.gov.

by attaching a paramagnetic label to a surface engineered cysteine via disulfide chemistry). Because the magnetic moment of an unpaired electron is very large, the PRE effect is measurable out to long paramagnetic center-proton distances.

2. Paramagnetic labels for PRE measurements.

In the case of PRE measurements it is important to employ paramagnetic labels with an isotropic *g*-tensor (6). This eliminates pseudo-contact shifts and minimizes Curie spin-relaxation. There are generally two classes of paramagnetic labels: the first is based on nitroxide free radicals (14), the second on suitable metal ions, such as Mn^{2+}, Cu^{2+} or Gd^{3+}, chelated to EDTA (15). In both instances, site-directed spin-labeling of proteins is generally achieved by conjugating the paramagnetic tag to a surface-exposed cysteine residue introduced by site-specific mutagenesis, making use of a methanethiosulfonate or pyridylthiol functional group to form a disulfide link between the cysteine and the paramagnetic tag (16). Alternatives to the use of disulfide chemistry include the addition of short metal-binding sequences to the protein of interest; for example the N-terminal ATCUN motif (XXH) binds Cu^{2+} (17) and the N-terminal HHP sequences forms a dimer between two peptides bound to Ni^{2+} (18).

The linker connecting the surface cysteine with the paramagnetic label usually has several rotatable bonds. As a result, the paramagnetic center can sample a substantial amount of conformational space which has to be taken into account when interpreting PRE data quantitatively. There are paramagnetic labels where the conformational space is more restricted: examples include the R1p side chain (19), a 4-pyridyl analog of the R1 side chain, and a caged lanthanide probe CLaNP which is attached to the protein via two cysteines (20, 21).

3. Measurement of the PRE

The PRE is measured by taking the difference in nuclear relaxation rates between the paramagnetic sample and a diamagnetic control (e.g. Mn^{2+} versus Ca^{2+} in the case of EDTA conjugates). While both longitudinal (Γ_1) and transverse (Γ_2) PRE rates can be measured, it is generally the case that measurements of Γ_2 provide the most reliable and accurate data (6, 22, 23). The reasons for this are several-fold. First, cross-relaxation and hydrogen exchange with water molecules reduce the accuracy of Γ_1 measurements (24). Second, in systems with an isotropic *g* tensor, the contribution of Curie-spin relaxation to Γ_2 is negligible and Γ_2 is dominated by direct dipole-dipole interactions between the unpaired electrons of the paramagnetic tag and the nuclei of interest. As a result Γ_2 does not exhibit cross-correlation with other relaxation mechanisms. Third, since there are no pseudo-contact shifts in isotropic systems, the exchange contributions to R_2 are identical for the paramagnetic and diamagnetic states and are therefore canceled out when Γ_2 is measured by taking the difference in R_2 between the paramagnetic sample and the diamagnetic control. And fourth, Γ_2 is minimally impacted by fast internal motions, whereas Γ_1 is very sensitive to them.

Many PRE studies in the literature make use of a simplistic approach in which the ratio of peak intensities in a 2D correlation spectrum between paramagnetic and diamagnetic

samples is used as a measure of the PRE. Determination of Γ_2 values from these ratios requires knowledge of the R_2 values in the diamagnetic state, the use of sufficiently long repetition delays between scans to ensure that magnetization recovery levels are identical for the paramagnetic and diamagnetic states, the assumption of Lorentzian lineshapes, and absolutely identical concentrations for the paramagnetic and diamagnetic samples (23). For a deuterated protein, the amide ^1H_N-T_1 relaxation time is very long and interscan delays in excess of 20 s may be required; the assumption of Lorentzian line-shapes precludes the use of all window functions other than an exponential, and hence is not suitable for systems with any significant degree of spectral complexity and cross-peak overlap; and finally it is virtually impossible to ensure equal concentrations for two separate samples. All these issues are readily overcome by measuring R_2 directly from a two-time point measurement, thereby enabling the direct determination of Γ_2 values and their associated errors without making use of any fitting procedures (22, 23). Especially important is the fact that the two-time point approach does not require identical sample concentrations for the paramagnetic and diamagnetic states, nor does it necessitate the use of long interscan delays. As a result, quantitative measurement of Γ_2 using the two-time point approach is not only far more accurate but is also actually significantly faster than the single time point measurement (23).

Two-time point measurements of R_2 rates can be accomplished by a variety of 2D or 3D heteronuclear correlation-based experiments using either conventional heteronuclear single quantum correlation (HSQC) or transverse optimized (TROSY) correlation spectroscopy (23, 25).

4. Using the PRE in structure determination

Early work using PREs for structure determination converted the PRE data into very approximate distance restraints with wide error ranges (26–29). While approximate distance restraints derived from NOE data are very effective since a restraint of say less than 6 Å between two protons that could potentially be 100 Å apart obviously places severe constraints on the conformational space consistent with the data. However, a PRE-derived restraint of say 20±10 Å is obviously much less constraining. Effective use of PRE data in structure determination therefore requires direct refinement against the PRE data (22). To do this properly, several considerations have to be taken into account (22). First, as the paramagnetic label is generally not rigid and can sample a large region of conformational space, Γ_2 is an ensemble-averaged quantity related to the $\langle r^{-6} \rangle$ average of the electron-proton distance. Consequently, the paramagnetic label must be represented by an ensemble of states in any calculation. Practical experience indicates that a conformational ensemble with between 3 and 6 members is more than sufficient for this purpose. The second consideration is that the mobility of the paramagnetic label has to be taken into account which requires extension of the Solomon-Bloembergen (SB) theory of the PRE (30) (31) to a model free formalism (referred to a SBMF) in which order parameters from the electron-proton vectors are calculated on the fly from the coordinates during the course of the structure calculations (22). Readily available simulated annealing structure determination protocols incorporating the SBMF framework have been implemented in Xplor-NIH (32).

An example of a structure of a protein-DNA complex involving the male sex determining factor SRY determined from backbone amide and methyl proton PRE measurements using a DNA duplex labeled at three sites (individually) with dT-EDTA-Mn^{2+} is shown in Fig. 1 (22).

5. Using the PRE to detect transient sparsely-populated states.

If two states exchange with one another, the PREs from the minor state can leave their footprint on the PREs measured on the observable major state providing two conditions are fulfilled (6, 7, 13): first, and most importantly, the paramagnetic center-proton distances in the minor state must be shorter than in the major state; and second, the overall interconversion rate (k_{ex}) between the two species must be fast enough to permit the transfer of PREs from the minor state to the observable major state. This is illustrated in Fig. 2. If exchange is slow on the PRE time scale, (i.e.$\Gamma_2^{minor} - \Gamma_2^{major} \ll k_{ex}$), only the major species will contribute to the observed PRE; if on the other hand, exchange is fast on the PRE time scale (i.e.$\Gamma_2^{minor} - \Gamma_2^{major} \gg k_{ex}$) then the observed PRE measured on the major species will be a populated weighted average of the PREs in the major and minor states. If one considers a system in which a given paramagnetic center-proton distance varies from 30 Å in the major species to 8 Å in the minor one, this can translate into a substantial apparent PRE measured on the spectrum of the major species.

This effect was initially discovered by accident while carrying out PRE measurements on a tight (K_D ~ 1 nM) specific complex of the transcription factor HoxD9 with DNA in which the DNA was paramagnetically tagged at several sites with dT-EDTA-Mn^{2+} (7). At low salt (20 mM NaCl), all the PREs could be accounted for by the known crystal structure of the specific complex; but at higher salt concentrations (100–150 mM NaCl), PREs were observed at proton sites on the protein that were distant from the paramagnetic tags in the structure of the specific complex. These PREs were shown to arise from a combination of intramolecular sliding of HoxD9 along the DNA as well as from direct intermolecular translocation of HoxD9 between DNA molecules (without dissociating into free solution). Subsequently, PREs arising from minor states with occupancies as low as 0.5% have been used to probe transient encounter complexes in protein-protein association (8, 9, 11, 33) and conformational sampling of domains in multidomain proteins (10, 25).

An example of the use of PREs to explore the conformational space sampled by sparsely-populated states of a protein is illustrated with calmodulin (CaM-4Ca^{2+}) in Fig. 3 (25). CaM-4Ca^{2+} has two domains connected by a linker; in the absence of a target peptide the two domains reorient semi-independently of one another, but clamp down upon binding to a target peptide to form a compact globular structure in which the two domains envelope the peptide. No NOEs are observed between the two domains of CaM-4Ca^{2+}. When CaM-4Ca^{2+} is paramagnetically tagged at either the N- or C-terminal domains with a nitroxide label, the intradomain PRE profiles are consistent with the domain structures in the absence and presence of target peptide (Fig. 3A); however, whereas the interdomain PRE profiles obtained in the presence of the target peptide from myosin light chain kinase (MLCK) are fully accounted for by the structure of CaM-4Ca^{2+}-MLCK complex (34, 35) (panels 1 and 3

of Fig. 3A), those obtained in the absence of target peptide are not consistent with either the crystal structure of CaM-4Ca^{2+} (which predicts that no intermolecular PREs should be observed) (36) or the structure of the CaM-4Ca^{2+}-MLCK complex (panels 2 and 4 of Fig. 3 A). The observed interdomain PREs for CaM-4Ca^{2+} are indicative of the existence of transient sparsely-populated closed conformations in which the N- and C-terminal domains of CaM come into close proximity to one another. Using PRE-driven simulated annealing it was shown that the population of such closed states is about 10% (Fig. 3B), and the majority (about half) of these states sample a region of conformational space that closely overlaps that found in various crystal structures CaM-4Ca^{2+}-peptide complexes (Fig. 3C). Thus, even in the absence of target peptide there exists a small population of closed or partially-closed states that are similar but not identical to the closed states observed in complexes with target peptides. The population of the partially closed states correlates with linker length between the two domains as well as with the affinity of CaM-4Ca^{2+} for target peptide (37). These results highlight the complementarity and interplay of conformational selection and induced fit in ligand binding, and suggest that the existence of a small population of partially-closed states in the absence of ligand may facilitate the transition to the full closed ligand-bound state (38).

ACKNOWLEDGEMENTS

This work was supported by the Intramural Program of the National Institute of Diabetes and Digestive and Kidney Diseases at the National Institutes of Health, and by the AIDS Targeted Antiviral Program of the Office of the Director of the National Institutes of Health

REFERENCES

1. Clore GM & Gronenborn AM (1989) Determination of three-dimensional structures of proteins and nucleic acids in solution by nuclear magnetic resonance spectroscopy. Critical Reviews in Biochemistry and Molecular Biology 24(5), 479–564. [PubMed: 2676353]
2. Clore GM & Gronenborn AM (1998) New methods of structure refinement for macromolecular structure determination by NMR. Proceedings of the National Academy of Sciences of the United States of America 95(11), 5891–5898. [PubMed: 9600889]
3. Clore GM & Gronenborn AM (1998) Determining the structures of large proteins and protein complexes by NMR. Trends in Biotechnology 16(1), 22–34. [PubMed: 9470228]
4. Clore GM & Venditti V (2013) Structure, dynamics and biophysics of the cytoplasmic protein-protein complexes of the bacterial phosphoenolpyruvate: sugar phosphotransferase system. Trends in Biochemical Sciences 38(10), 515–530. [PubMed: 24055245]
5. Bax A & Grishaev A (2005) Weak alignment NMR: a hawk-eyed view of biomolecular structure. Current Opinion in Structural Biology 15(5), 563–570. [PubMed: 16140525]
6. Clore GM & Iwahara J (2009) Theory, practice, and applications of paramagnetic relaxation enhancement for the characterization of transient low-population states of biological macromolecules and their complexes. Chemical Reviews 109(9), 4108–4139. [PubMed: 19522502]
7. Iwahara J & Clore GM (2006) Detecting transient intermediates in macromolecular binding by paramagnetic NMR. Nature 440(7088), 1227–1230. [PubMed: 16642002]
8. Tang C, Iwahara J, & Clore GM (2006) Visualization of transient encounter complexes in protein-protein association. Nature 444(7117), 383–386. [PubMed: 17051159]
9. Volkov AN, Worrall JA, Holtzmann E, & Ubbink M (2006) Solution structure and dynamics of the complex between cytochrome c and cytochrome c peroxidase determined by paramagnetic NMR. Proceedings of the National Academy of Sciences of the United States of America 103(50), 18945–18950. [PubMed: 17146057]

10. Tang C, Schwieters CD, & Clore GM (2007) Open-to-closed transition in apo maltose-binding protein observed by paramagnetic NMR. Nature 449(7165), 1078–1082. [PubMed: 17960247]
11. Tang C, Louis JM, Aniana A, Suh JY, & Clore GM (2008) Visualizing transient events in amino-terminal autoprocessing of HIV-1 protease. Nature 455(7213), 693–696. [PubMed: 18833280]
12. Clore GM, Tang C, & Iwahara J (2007) Elucidating transient macromolecular interactions using paramagnetic relaxation enhancement. Current Opinion in Structural Biology 17(5), 603–616. [PubMed: 17913493]
13. Anthis NJ & Clore GM (2015) Visualizing transient dark states by NMR spectroscopy. Quarterly Reviews of Biophysics 48(1), 35–116. [PubMed: 25710841]
14. Kosen PA (1989) Spin labeling of proteins. Methods in Enzymology 177(86–121. [PubMed: 2558275]
15. Iwahara J, Anderson DE, Murphy EC, & Clore GM (2003) EDTA-derivatized deoxythymidine as a tool for rapid determination of protein binding polarity to DNA by intermolecular paramagnetic relaxation enhancement. Journal of the American Chemical Society 125(22), 6634–6635. [PubMed: 12769564]
16. Altenbach C, Marti T, Khorana HG, & Hubbell WL (1990) Transmembrane protein structure: spin labeling of bacteriorhodopsin mutants. Science 248(4959), 1088–1092. [PubMed: 2160734]
17. Mal TK, Ikura M, & Kay LE (2002) The ATCUN domain as a probe of intermolecular interactions: Application to calmodulin-peptide complexes. Journal of the American Chemical Society 124(47), 14002–14003. [PubMed: 12440892]
18. Jensen MR, Lauritzen C, Dahl SW, Pedersen J, & Led JJ (2004) Binding ability of a HHP-tagged protein towards Ni^{2+} studied by paramagnetic NMR relaxation: The possibility of obtaining long-range structure information. Journal of biomolecular NMR 29(3), 465–465.
19. Fawzi NL, et al. (2011) A rigid disulfide-linked nitroxide side chain simplifies the quantitative analysis of PRE data. Journal of biomolecular NMR 51(1–2), 105–114. [PubMed: 21947919]
20. Keizers PHJ, Desreux JF, Overhand M, & Ubbink M (2007) Increased paramagnetic effect of a lanthanide protein probe by two-point attachment. Journal of the American Chemical Society 129(30), 9292–9293. [PubMed: 17608481]
21. Keizers PHJ, Saragliadis A, Hiruma Y, Overhand M, & Ubbink M (2008) Design, Synthesis, and Evaluation of a Lanthanide Chelating Protein Probe: CLaNP-5 Yields Predictable Paramagnetic Effects Independent of Environment. Journal of the American Chemical Society 130(44), 14802–14812. [PubMed: 18826316]
22. Iwahara J, Schwieters CD, & Clore GM (2004) Ensemble approach for NMR structure refinement against (1)H paramagnetic relaxation enhancement data arising from a flexible paramagnetic group attached to a macromolecule. Journal of the American Chemical Society 126(18), 5879–5896. [PubMed: 15125681]
23. Iwahara J, Tang C, & Clore GM (2007) Practical aspects of ^{1}H transverse paramagnetic relaxation enhancement measurements on macromolecules. Journal of Magnetic Resonance 184(2), 185–195. [PubMed: 17084097]
24. Iwahara J & Clore GM (2010) Structure-independent analysis of the breadth of the positional distribution of disordered groups in macromolecules from order parameters for long, variable-length vectors using NMR paramagnetic relaxation enhancement. Journal of the American Chemical Society 132(38), 13346–13356. [PubMed: 20795737]
25. Anthis NJ, Doucleff M, & Clore GM (2011) Transient, sparsely populated compact states of apo and calcium-loaded calmodulin probed by paramagnetic relaxation enhancement: interplay of conformational selection and induced fit. Journal of the American Chemical Society 133(46), 18966–18974. [PubMed: 21999431]
26. Schmidt PG & Kuntz ID (1984) Distance measurements in spin-labeled lysozyme. Biochemistry 23(18), 4261–4266. [PubMed: 6091743]
27. Kosen PA, et al. (1986) Two-dimensional ^{1}H NMR of three spin-labeled derivatives of bovine pancreatic trypsin inhibitor. Biochemistry 25(9), 2356–2364. [PubMed: 2424497]
28. Battiste JL & Wagner G (2000) Utilization of site-directed spin labeling and high-resolution heteronuclear nuclear magnetic resonance for global fold determination of large proteins with limited nuclear overhauser effect data. Biochemistry 39(18), 5355–5365. [PubMed: 10820006]

29. Gaponenko V, et al. (2000) Protein global fold determination using site-directed spin and isotope labeling. Protein Science 9(2), 302–309. [PubMed: 10716182]
30. Solomon I (1955) Relaxation Processes in a System of 2 Spins. Physical Review 99(2), 559–565.
31. Bloembergen N & Morgan LO (1961) Proton Relaxation Times in Paramagnetic Solutions Effects of Electron Spin Relaxation. Journal of Chemical Physics 34(3), 842-&.
32. Schwieters CD, Kuszewski JJ, & Clore GM (2006) Using Xplor-NIH for NMR molecular structure determination. Progress in Nuclear Magnetic Resonance Spectroscopy 48(1), 47–62.
33. Fawzi NL, Doucleff M, Suh JY, & Clore GM (2010) Mechanistic details of a protein-protein association pathway revealed by paramagnetic relaxation enhancement titration measurements. Proceedings of the National Academy of Sciences of the United States of America 107(4), 1379–1384. [PubMed: 20080627]
34. Ikura M, et al. (1992) Solution structure of a calmodulin-target peptide complex by multidimensional NMR. Science 256(5057), 632–638. [PubMed: 1585175]
35. Meador WE, Means AR, & Quiocho FA (1992) Target enzyme recognition by calmodulin: 2.4 Å structure of a calmodulin-peptide complex. Science 257(5074), 1251–1255. [PubMed: 1519061]
36. Babu YS, et al. (1985) Three-dimensional structure of calmodulin. Nature 315(6014), 37–40. [PubMed: 3990807]
37. Anthis NJ & Clore GM (2013) The length of the calmodulin linker determines the extent of transient interdomain association and target affinity. Journal of the American Chemical Society 135(26), 9648–9651. [PubMed: 23782151]
38. Clore GM (2014) Interplay between conformational selection and induced fit in multidomain protein-ligand binding probed by paramagnetic relaxation enhancement. Biophysical Chemistry 186, 3–12. [PubMed: 24070540]

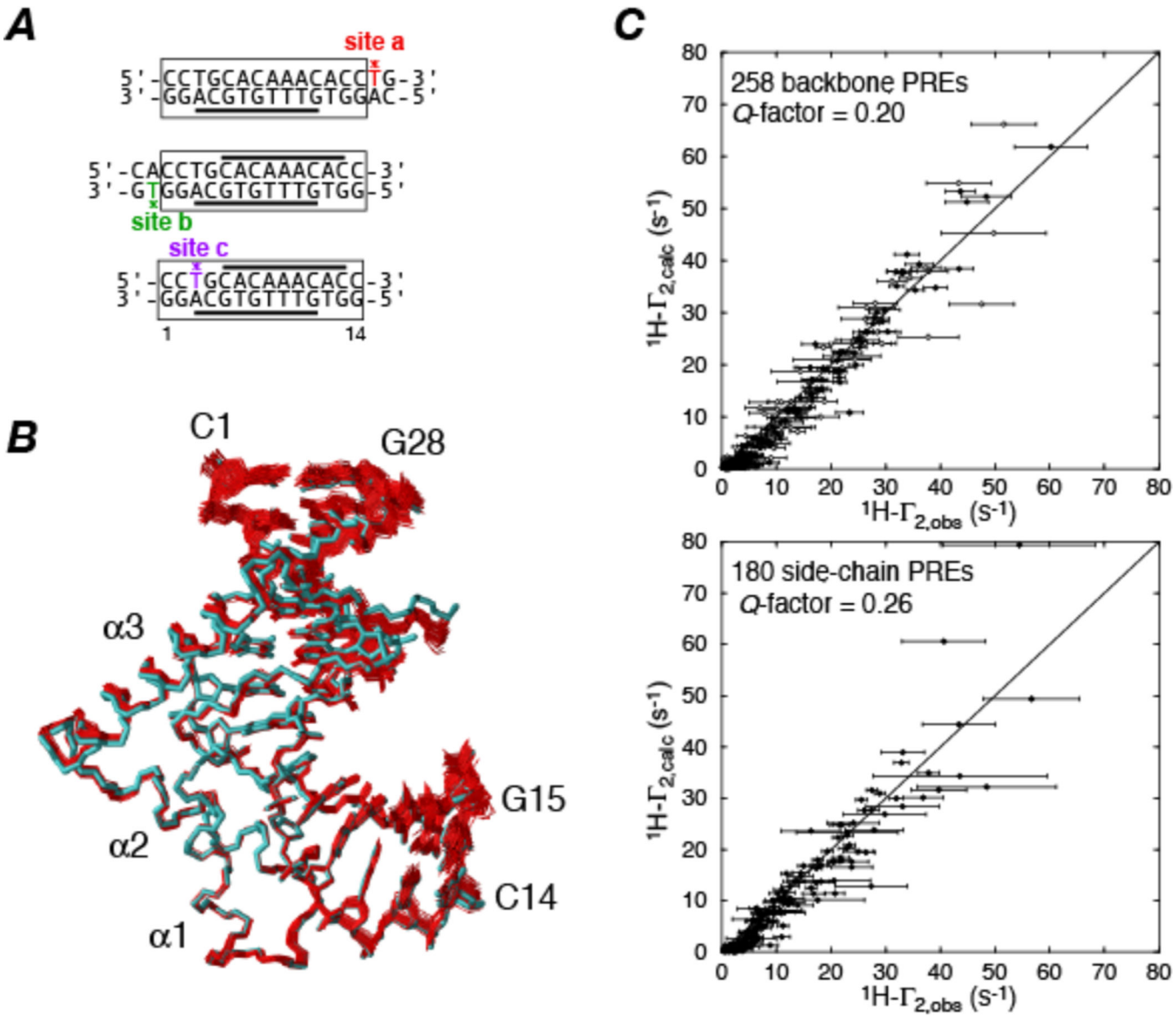

Figure 1.

Refinement of the SRY-DNA complex using intermolecular PREs. (A) Paramagnetically-labeled dT-EDTA-Mn^{2+} DNA duplexes used to measure intermolecular PREs on $^{15}N/^{13}C$-labeled SRY. The positions of the paramagnetic tags are indicated by asterisks. (B) Superposition of 40 simulated annealing structures refined against 438 ^{1}H intermolecular PRE restraints (red) superimposed on the regularized mean structure obtained from NOE, torsion angle, ^{3}J coupling and residual dipolar coupling restraints. (C) Correlation between observed and calculated PREs for backbone amide (top) and side chain (bottom) protons. The quality of agreement between experimental (Γ_2^{obs}) and calculated (Γ_2^{calc}) values is calculated by a Q-factor given by $\sqrt{\{\sum_i [\Gamma_2^{obs}(i) - \Gamma_2^{calc}(i)]^2\} / \sum_i \Gamma_2^{obs}(i)^2}$ Adapted from ref. (22).

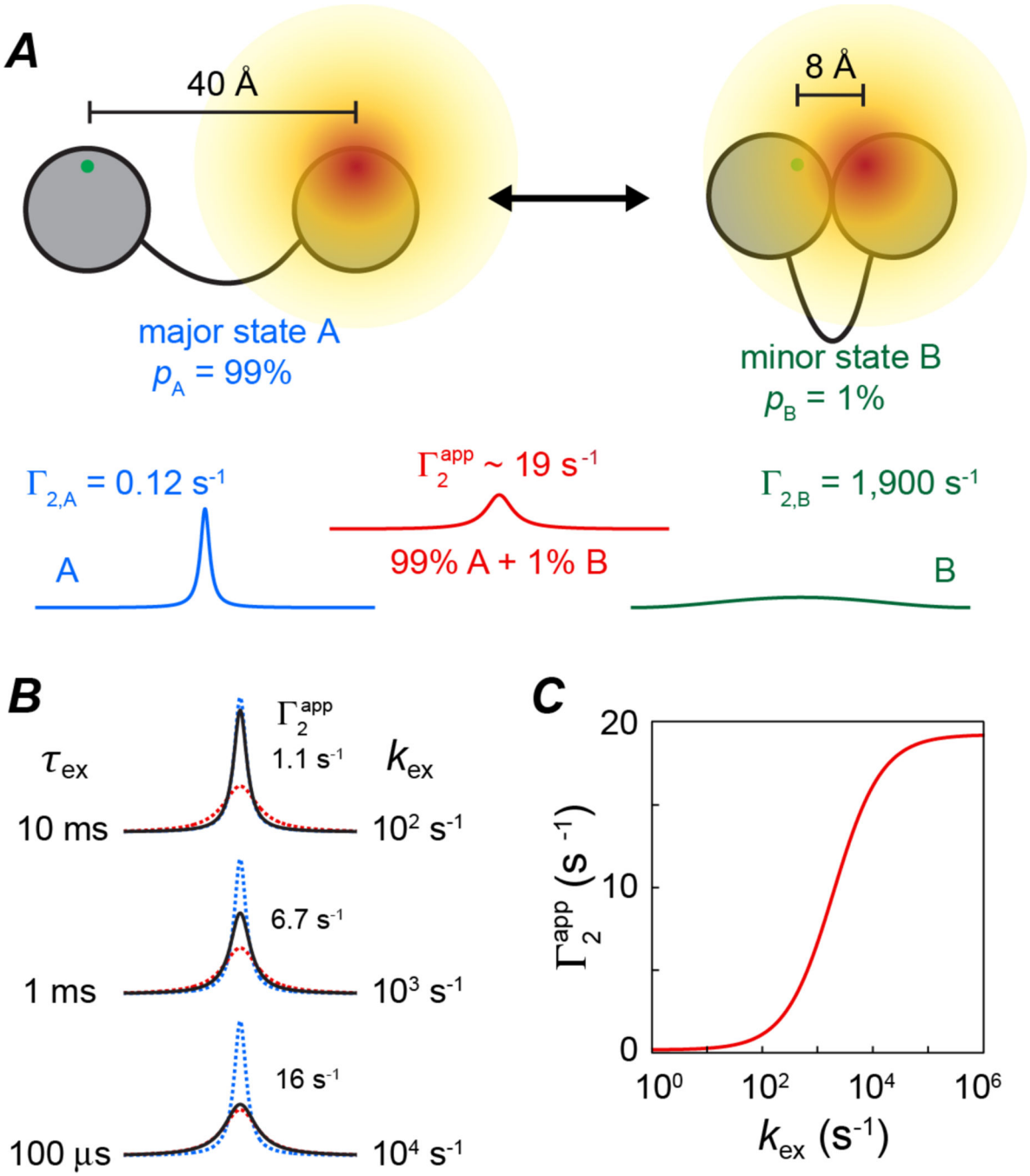

Figure 2.

Basis of using PREs to detect sparsely-populated states. (A) The unpaired electron of the paramagnetic label and the proton of interest are depicted as green and red dots on two separated domains of a protein. In the major species A (populated at 99%) the unpaired electron-proton distance is 40 Å but reduced to 8 Å in the minor species B (populated at 1%). For a nitroxide spin label these distances correspond to Γ_2 PRE values of 0.12 and 1900 s^{-1}, respectively. If states A and B are in slow exchange on the PRE time scale, the observed transverse relaxation rates $R_{2,i}^{obs}$ for a given species will be the sum of its intrinsic

transverse relaxation rate $R_{2,i}^{\text{intrinsic}}$ and $\Gamma_{2,i}$, resulting in a narrow linewidth for the resonance of species A (blue) but a line broadened beyond detection for species B (green, which is already undetectable owing to its low population). In the fast exchange limit, a single resonance will be observed at the position of species A, line broadened by the apparent $\Gamma_2\left(\Gamma_2^{\text{app}}\right)$ given by the population-weighted average of the Γ_2 values of species A and B (red line) (B) Impact of exchange (expressed as a lifetime $\boldsymbol{\tau}_{\text{ex}}$ on the left and an exchange rate k_{ex} on the right) on the observed linewidth (black) of the resonance of species A; the resonance of species A in the absence of exchange and in the fast-exchange limit are depicted by the blue and red dashed lines, respectively. (C) Dependence of Γ_2^{app} on k_{ex}. Adapted from ref. (13).

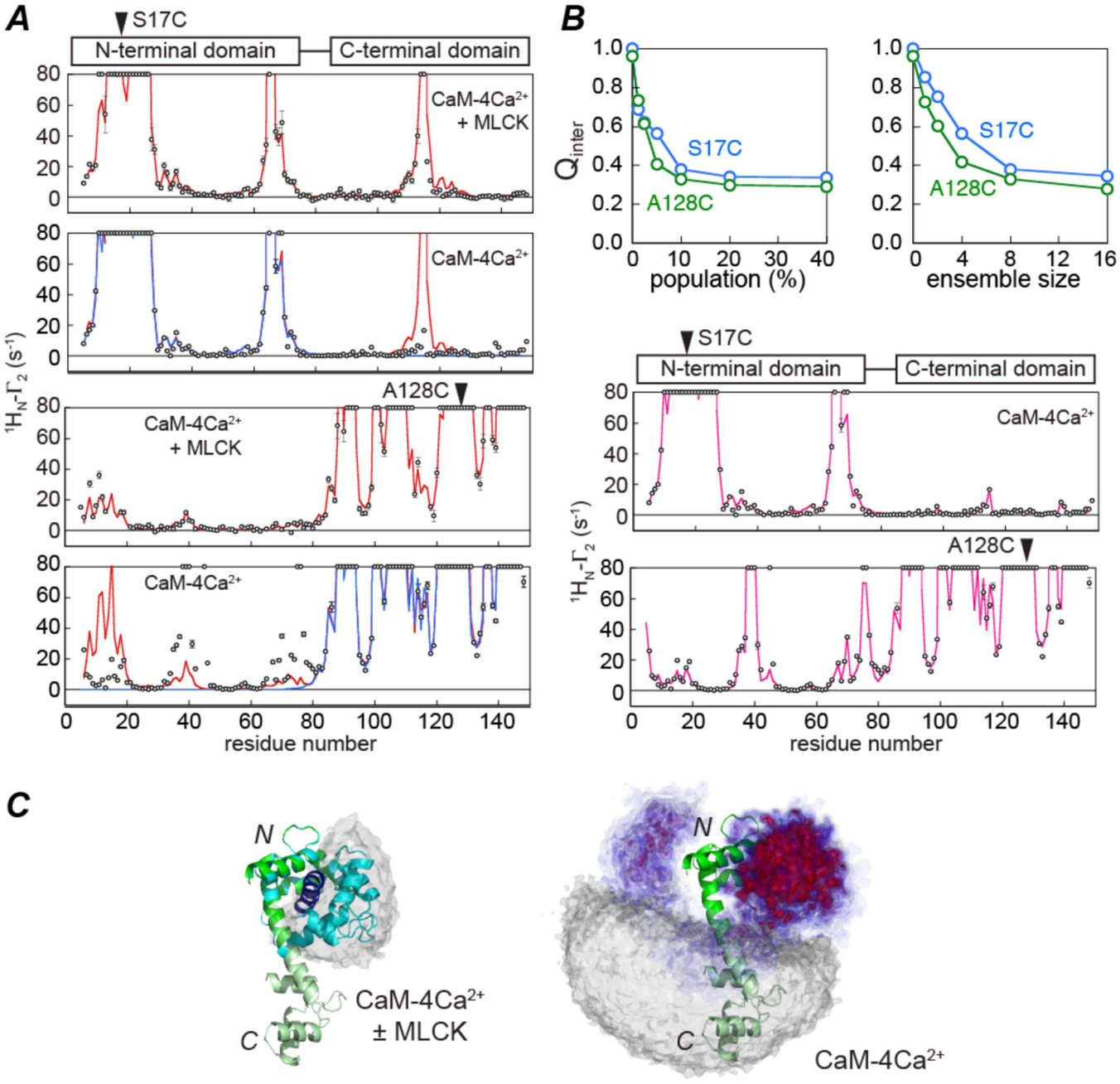

Figure 3.

Exploring the conformational space sampled by transient sparsely-populated closed states of calmodulin (CaM)-4Ca^{2+} from interdomain PRE data. (A) Observed (circles) and calculated PRE profiles (lines) observed for CaM-4Ca^{2+} in the presence (panels 1 and 3) and absence (panels 2 and 4) of the myosin light chain kinase (MLCK) target peptide. The paramagnetic nitroxide label is attached to S17C in panels 1 and 2 and to A128C in panels 3 and 4. Excellent agreement is obtained for the intradomain PREs in the presence and absence of the MLCK peptide. However, whereas the experimental interdomain PRE profiles obtained in the presence of the MLCK peptide agree well with those back-calculated from the crystal

structure of the CaM-4Ca^{2+}-MLCK complex (red line), those in the absence of peptide do not agree with the back-calculated PREs derived from the crystal structures of either CaM-4Ca^{2+} (blue) or CaM-4Ca^{2+}-MLCK (red). (B) PRE-driven simulated annealing refinement of CaM-4Ca^{2+}. The top panels show the dependence of the PRE Q-factor on the population of closed states and on the ensemble size used to represent the sparsely-populated species. The bottom two panels show the agreement between observed (circles) and calculated (red lines) PRE data. (C) Visualization of the conformational space sampled by sparsely-populated closed states of CaM-4Ca^{2+}. For reference the dumbbell crystal structure of CaM-4Ca^{2+} (36) is shown as a ribbon diagram with the N- and C-terminal domains shown in dark and light green, respectively; a ribbon of the C-terminal domain in the CaM-4Ca^{2+}-MLCK structure (35) is depicted in blue, and on the left panel the grey atomic probability map depicts the location of the C-terminal domain (relative to a fixed N-terminal domain) in a variety of CaM-peptide complex (25). On the left panel, the conformational space sampled by the C-terminal domain (relative to a fixed N-terminal domain) in the minor (~10%) closed species of CaM-4Ca^{2+} is depicted by an atomic probability map plotted at contour levels ranging from 0.1 (blue) to 0.5 (red); the grey probability map depicts the region of conformational space consistent with interdomain Γ_2 values less than 2 s^{-1} and is representative of the major species ensemble. The predominant region of conformational space (red probability map) sampled by the transient closed states of CaM-4Ca^{2+} overlaps with that sampled in the CaM-peptide complexes. Adapted from ref. (25).